Proceedings of Global Power and Propulsion Society
ISSN-Nr: 2504-4400
Beijing Conference 2019
16th – 18th September, 2019
www.gpps.global

GPPS-BJ-2019-0073

Study on acoustic-intrinsic thermoacoustic feedback on swirling flame combustors

Yong Chen
College of Aerospace Science and Engineering
literature_chen@nudt.edu.cn
Changsha, Hunan, China

ABSTRACT

This paper investigates the intrinsic thermoacoustic feedback and its interaction with the cavity acoustic resonations in swirling flame combustors. The dynamics of acoustic-vortical-entropic perturbations due to the unsteady heat release rate in a swirling flame is given where the azimuthal and axial base flow velocities are present. The critical gain of the intrinsic thermoacoustic (ITA) oscillation is given meanwhile parametric analysis shows that the difference of the transit time between acoustic and vortical perturbations play an important role on the ITA critical gain. Applied to the verification of experimental results of a swirling flame combustor, the present work predicts correctly the thermoacoustic oscillations. Analysis on the interaction between the intrinsic thermoacoustic feedback and the traditional cavity acoustic resonation feedback shows that the thermoacoustic modes of the whole system are composed of both flame-induced modes and the cavity acoustic modes. The flame dynamics seems to be able to construct a virtual cavity feedback in the absence of acoustic feedbacks from the boundary conditions. The increase of the transit time difference between the acoustic and vortical perturbations before the flame front reduces the frequencies of flame-induced modes and worsens their stabilities. The cavity acoustic mode, on the other hand, forms a periodic orbit and approaches to the orbit's attractor.

INTRODUCTION

Thermoacoustic instabilities, which arise from positive feedback between the unsteady heat release of the flame and flow perturbations-in particular acoustic waves-in a combustor, may cause problems from increased noise emissions to severe damage to engines ([1, 2]). They are commonly characterized as acoustic features of the combustion system driven by unsteady heat release of the flame, which feeds perturbation energy into acoustic cavity-oriented resonant modes ([3, 4]). However, recent research, including theoretical modelling ([5-8]), numerical simulations ([9, 10]) and experimental verifications ([11-13]), show that thermoacoustic instability can occur even in a fully anechoic environment where acoustic reflections from the inlet or outlet of the combustor are not involved. Due to their independence on chamber acoustic resonant behavior, they are often identified as intrinsic thermoacoustic (ITA) instability.

Hoeijmakers et al. [5] and Emmert et al. [6] independently gave theoretical analysis of ITA feedback of premixed flames in longitudinal combustions based on the low frequency acoustic network where the vortical perturbation is absent. Numerical simulations of intrinsic instabilities of laminar flames with non-reflecting boundary conditions confirm theoretical results ([9, 10]). ITA feedback have also been found in the practical combustor configurations with acoustic losses[7] or partially reflecting boundaries[14]. Recently, ITA modes were reported to be dominant in a perfectly premixed combustion system[15] and partially premixed turbulent combustion system[16]. In a Rijke burner, Hosseini et al. [13] analysed the interactions between the ITA modes and acoustic modes.

The above-mentioned contributions are based on the low frequency network where only the acoustic and entropic perturbations are considered. However, in many situations, a swirling flames exist[17], where a vortical perturbation is present and plays an important role on the flame[18]. As the ITA feedback is principally determined by the flame dynamics, it is of great interest to analyse the ITA mechanisms and the interactions of ITA modes and cavity acoustic modes in swirling flame combustors.

Based on the configuration of experimental test rig by Palies et al. [19] and Silva et al. [20], the present paper therefore investigates the ITA mechanism as well as their interactions with acoustic modes. Mathematical formulation of the acoustic-vortical-entropic perturbations in a swirling flame is given in Section 2. Section 3 presents the derivation and parametric analysis of the critical gain of ITA oscillation. Section 4 analyses the interaction of ITA and acoustic modes

based on the experimental configuration. Section 5 concludes the work presented in this paper.

AZIMUTHAL PERTURBATION MODELLING AFFECTED BY UNSTEADY HEAT RELEASE

This section deals with the azimuthal perturbation dynamics of the unsteady heat release rate for a swirling flame as shown in Fig. 1. Parameters at the downstream and upstream of the flame front are denoted by superscripts 'd' and 'u' respectively. The fluid thermodynamics are characterized by the pressure p, temperature T and density ρ. The cross-sectional area is denoted by C. We assume there are axial (v^x) and azimuthal (v^θ) velocity components, then the velocity vector can be denoted by $\mathbf{v}=\left[0,v^\theta,v^x\right]$. The entropy and vortices are denoted by s and ϖ. The steady and linear perturbation components are denoted by '-' and '′'.

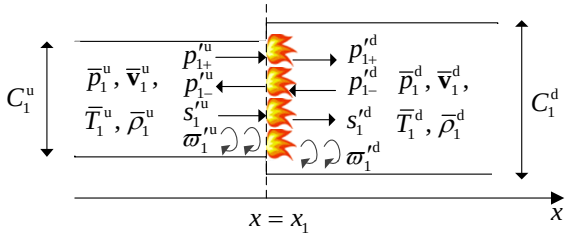

Fig. 1. Schematic diagram of azimuthal perturbation dynamics for a swirling flame

Based on the work of Stow and Dowling [21] and LeVeque [22], conservations of mass, axial momentum, angular momentum and energy, in the low Mach number approximation, across the flame front can be expressed by

$$\begin{aligned}
&C_1^{\mathrm{d}}\bar{\rho}_1^{\mathrm{d}}\left(\bar{v}_1^x\right)^{\mathrm{d}}-C_1^{\mathrm{u}}\bar{\rho}_1^{\mathrm{u}}\left(\bar{v}_1^x\right)^{\mathrm{u}}=0,\\
&C_1^{\mathrm{d}}\bar{p}_1^{\mathrm{d}}-C_1^{\mathrm{u}}\bar{p}_1^{\mathrm{u}}-\left(C_1^{\mathrm{d}}-C_1^{\mathrm{u}}\right)\Lambda_1^{\mathrm{u}}\bar{p}_1^{\mathrm{u}}=0,\\
&R_1^{\mathrm{d}}\left(\bar{v}_1^\theta\right)^{\mathrm{d}}-R_1^{\mathrm{u}}\left(\bar{v}_1^\theta\right)^{\mathrm{u}}=0,\\
&\frac{\gamma}{\gamma-1}\left(C_1^{\mathrm{d}}\bar{p}_1^{\mathrm{d}}\left(\bar{v}_1^x\right)^{\mathrm{d}}-C_1^{\mathrm{u}}\bar{p}_1^{\mathrm{u}}\left(\bar{v}_1^x\right)^{\mathrm{u}}\right)=\bar{\dot{Q}},
\end{aligned}\tag{1}$$

where $\int_{C_1^{\mathrm{u}}}^{C_1^{\mathrm{d}}}\bar{p}\mathrm{d}C=\left(C_1^{\mathrm{d}}-C_1^{\mathrm{u}}\right)\Lambda_1^{\mathrm{u}}\bar{p}_1^{\mathrm{u}}$ is used and γ is the heat capacity ratio. Meanwhile the governing equations of the linear perturbation for the low Mach number are

conservation of mass

$$\frac{\hat{\rho}_1^{\mathrm{d}}}{\bar{\rho}_1^{\mathrm{d}}}-\frac{\hat{\rho}_1^{\mathrm{u}}}{\bar{\rho}_1^{\mathrm{u}}}+\frac{\left(\hat{v}_1^x\right)^{\mathrm{d}}}{\left(\bar{v}_1^x\right)^{\mathrm{d}}}-\frac{\left(\hat{v}_1^x\right)^{\mathrm{u}}}{\left(\bar{v}_1^x\right)^{\mathrm{u}}}=0,\tag{2}$$

conservation of axial momentum

$$\frac{\hat{p}_1^{\mathrm{d}}}{\gamma\bar{p}_1^{\mathrm{d}}}=\left[1+\left(1-\frac{1}{\alpha_1^{\mathrm{u}}}\right)\left(\Gamma_1^{\mathrm{u}}(\omega)-\Lambda_1^{\mathrm{u}}\right)\frac{\bar{p}_1^{\mathrm{u}}}{\bar{p}_1^{\mathrm{d}}}\right]\frac{\hat{p}_1^{\mathrm{u}}}{\gamma\bar{p}_1^{\mathrm{u}}},\tag{3}$$

conservation of azimuthal momentum

$$\frac{\left(\hat{v}_1^\theta\right)^{\mathrm{d}}}{\left(\bar{v}_1^\theta\right)^{\mathrm{d}}}=\frac{\left(\hat{v}_1^\theta\right)^{\mathrm{u}}}{\left(\bar{v}_1^\theta\right)^{\mathrm{u}}},\tag{4}$$

and conservation of energy

$$\begin{aligned}
\frac{\left(\hat{v}_1^x\right)^{\mathrm{d}}}{\left(v_1^x\right)^{\mathrm{d}}}&=\frac{1}{\lambda_1^{\mathrm{u}}}\frac{\left(\hat{v}_1^x\right)^{\mathrm{u}}}{\left(\bar{v}_1^x\right)^{\mathrm{u}}}+\left(1-\frac{1}{\lambda_1^{\mathrm{u}}}\right)\frac{\hat{\dot{Q}}}{\bar{\dot{Q}}}\\
&+\gamma\left[\left(\frac{1}{\lambda_1^{\mathrm{u}}}-1\right)+\left(\frac{1}{\alpha_1^{\mathrm{u}}}-1\right)\left(\Gamma_1^{\mathrm{u}}(\omega)-\Lambda_1^{\mathrm{u}}\right)\frac{\bar{p}_1^{\mathrm{u}}}{\bar{p}_1^{\mathrm{d}}}\right]\frac{\hat{p}_1^{\mathrm{u}}}{\gamma\bar{p}_1^{\mathrm{u}}}.
\end{aligned}\tag{5}$$

In the above equations, we introduce $\int_{C_1^{\mathrm{u}}}^{C_1^{\mathrm{d}}}\hat{p}\mathrm{d}C=\left(C_1^{\mathrm{d}}-C_1^{\mathrm{u}}\right)\Gamma_1^{\mathrm{u}}(\omega)\hat{p}_1^{\mathrm{u}}$, $\lambda_1^{\mathrm{u}}=\bar{T}_1^{\mathrm{d}}/\bar{T}_1^{\mathrm{u}}$ and $\alpha_1^{\mathrm{u}}=C_1^{\mathrm{d}}/C_1^{\mathrm{u}}$. The overscript '^' denotes the Fourier transformation of perturbations ($\partial/\partial t\sim\mathrm{i}\omega t$ with $\omega=2\pi f$ being the angular frequency).

We now consider the propagation of the unsteady perturbations, physically speaking, the acoustic perturbation can be propagated upstream and downstream while the entropic and vortical perturbations can only convect with the base flow. Using appendix A, we may write the equations governing the propagation of these disturbances as

$$\left[\frac{\hat{v}^x}{\bar{v}^x},\frac{\hat{p}}{\gamma\bar{p}},\frac{\hat{s}}{c_p},\frac{\hat{v}^\theta}{\bar{v}^\theta}\right]^T=\mathbf{F}(x)\left[\frac{P_+}{\gamma\bar{p}},\frac{P_-}{\gamma\bar{p}},\frac{S}{c_p},\frac{A}{\gamma\bar{p}}\right]^T,\tag{6}$$

with

$$\mathbf{F}(x)=\begin{bmatrix}
-\dfrac{k_+^{\mathrm{a}}\exp\left(\mathrm{i}k_+^{\mathrm{a}}x\right)}{\bar{M}^x\left(\omega^*/\bar{c}+M^xk_+^{\mathrm{a}}\right)} & -\dfrac{k_-^{\mathrm{a}}\exp\left(\mathrm{i}k_-^{\mathrm{a}}x\right)}{M^x\left(\omega^*/\bar{c}+M^xk_-^{\mathrm{a}}\right)} & 0 & \dfrac{m\exp\left(\mathrm{i}k^{\mathrm{v}}x\right)}{M^x}\\
\exp\left(\mathrm{i}k_+^{\mathrm{a}}x\right) & \exp\left(\mathrm{i}k_-^{\mathrm{a}}x\right) & 0 & 0\\
0 & 0 & \exp\left(\mathrm{i}k^{\mathrm{e}}x\right) & 0\\
-\dfrac{\bar{c}}{\bar{v}^\theta}\dfrac{m\exp\left(\mathrm{i}k_+^{\mathrm{a}}x\right)}{R\left(\omega^*/\bar{c}+M^xk_+^{\mathrm{a}}\right)} & -\dfrac{\bar{c}}{\bar{v}^\theta}\dfrac{m\exp\left(\mathrm{i}k_-^{\mathrm{a}}x\right)}{R\left(\omega^*/\bar{c}+M^xk_-^{\mathrm{a}}\right)} & 0 & -\dfrac{\bar{c}}{\bar{v}^\theta}Rk^{\mathrm{v}}\exp\left(\mathrm{i}k^{\mathrm{v}}x\right)
\end{bmatrix},$$

$\omega^*=\omega+m\bar{v}^\theta$ with $M^x=\bar{v}^x/\bar{c}$ with $\bar{c}$ and m being the adiabatic sound speed and the integer azimuthal wavenumber ($\exp(\mathrm{i}m\theta)$) respectively. Ignoring the azimuthal base velocity ($\bar{v}^\theta$), the above equation reduces to the model of Dowling and Mahmoudi [3]. In the above equations, P, S and A denote the amplitude of the acoustic, entropic and vortical perturbations. Meanwhile, the corresponding axial wavenumbers are

$$\bar{c}k_{+,-}^{\mathrm{a}}=\frac{\omega^*M^x\mp\sqrt{\omega^{*2}-\left(1-\left(M^x\right)^2\right)\left(\bar{c}m/R\right)^2}}{\left(1-\left(M^x\right)^2\right)},\ k^{\mathrm{e}}=k^{\mathrm{v}}=-\frac{\omega^*}{\bar{v}^x}.$$

According to the definition of the vortical perturbation ($\varpi' = \nabla \times \mathbf{v}'$), we have

$$\hat{\varpi}^r = \frac{\mathrm{i}}{R\bar{\rho}\bar{c}}\left[m^2 + \left(Rk^{\mathrm{v}}\right)^2\right] A\exp\left[\mathrm{i}\left(m\theta + k^{\mathrm{v}}x\right)\right], \hat{\varpi}^\theta = \hat{\varpi}^x = 0.$$

As we are interested in the generations of perturbations downstream due to the unsteady heat release rate, we first substitute Eq. (6) into Eq. (2) and obtain the equation of the generation of the downstream entropic perturbation

$$\frac{\hat{s}_1^{\mathrm{d}}}{c_p} = \left[\gamma\left(\frac{1}{\lambda_1^{\mathrm{u}}} - 1\right) + \left(1 - \frac{1}{\alpha_1^{\mathrm{u}}}\right)\left(\Gamma_1^{\mathrm{u}}(\omega) - \Lambda_1^{\mathrm{u}}\right)\frac{\bar{p}_1^{\mathrm{u}}}{\bar{p}_1^{\mathrm{d}}}(1-\gamma)\right]\frac{\hat{p}_1^{\mathrm{u}}}{\gamma\bar{p}_1^{\mathrm{u}}} + \left(\frac{1}{\lambda_1^{\mathrm{u}}} - 1\right)\frac{\left(\hat{v}_1^x\right)^{\mathrm{u}}}{\left(\bar{v}_1^x\right)^{\mathrm{u}}} + \frac{\hat{s}_1^{\mathrm{u}}}{c_p} + \left(1 - \frac{1}{\lambda_1^{\mathrm{u}}}\right)\frac{\hat{\bar{Q}}}{\bar{\dot{Q}}}. \quad (7)$$

Mathematically, Eqs. (2), (3), (4), (7) can be expressed in matrix form

$$\begin{bmatrix} \frac{\left(\hat{v}_1^{\mathrm{d}}\right)^x}{\left(\bar{v}_1^{\mathrm{d}}\right)^x} & \frac{\hat{p}_1^{\mathrm{d}}}{\gamma\bar{p}_1^{\mathrm{d}}} & \frac{\hat{s}_1^{\mathrm{d}}}{c_p} & \frac{\left(\hat{v}_1^{\mathrm{d}}\right)^\theta}{\left(\bar{v}_1^{\mathrm{d}}\right)^\theta} \end{bmatrix}^T = \mathbf{H}_1^{\mathrm{u}}\begin{bmatrix} \frac{\left(\hat{v}_1^{\mathrm{u}}\right)^x}{\left(\bar{v}_1^{\mathrm{u}}\right)^x} & \frac{\hat{p}_1^{\mathrm{u}}}{\gamma\bar{p}_1^{\mathrm{u}}} & \frac{\hat{s}_1^{\mathrm{u}}}{c_p} & \frac{\left(\hat{v}_1^{\mathrm{u}}\right)^\theta}{\left(\bar{v}_1^{\mathrm{u}}\right)^\theta} \end{bmatrix}^T + \mathbf{B}_Q\frac{\hat{\bar{Q}}}{\bar{\dot{Q}}}. \quad (8)$$

with $\mathbf{B}_Q = \begin{bmatrix} \left(1 - \frac{1}{\lambda_1^{\mathrm{u}}}\right) & 0 & \left(1 - \frac{1}{\lambda_1^{\mathrm{u}}}\right) & 0 \end{bmatrix}^T$ and

$$\mathbf{H}_1^{\mathrm{u}} = \begin{bmatrix} \frac{1}{\lambda_1^{\mathrm{u}}} & \left(\frac{1}{\lambda_1^{\mathrm{u}}} - 1\right)\gamma & 0 & 0 \\ 0 & 1 & 0 & 0 \\ \left(\frac{1}{\lambda_1^{\mathrm{u}}} - 1\right) & \left(\frac{1}{\lambda_1^{\mathrm{u}}} - 1\right)\gamma & 1 & 0 \\ 0 & 0 & 0 & 1 \end{bmatrix},$$

under the assumption of low Mach number condition where the perturbation due to the sudden duct expansion are be approximated as $\Gamma_1^{\mathrm{u}}(\omega) = \Lambda_1^{\mathrm{u}} = 1$ [23]. Substituting Eq. (6) into Eq. (8) gives

$$\mathbf{F}_1^{\mathrm{d}}(0)\left[\frac{P_{1+}^{\mathrm{d}}}{\gamma\bar{p}_1^{\mathrm{d}}}, \frac{P_{1-}^{\mathrm{d}}}{\gamma\bar{p}_1^{\mathrm{d}}}, \frac{S_1^{\mathrm{d}}}{c_p}, \frac{A_1^{\mathrm{d}}}{\gamma\bar{p}_1^{\mathrm{d}}}\right]^T = \mathbf{H}_1^{\mathrm{u}}\mathbf{F}_1^{\mathrm{u}}(0)\left[\frac{P_{1+}^{\mathrm{u}}}{\gamma\bar{p}_1^{\mathrm{u}}}, \frac{P_{1-}^{\mathrm{u}}}{\gamma\bar{p}_1^{\mathrm{u}}}, \frac{S_1^{\mathrm{u}}}{c_p}, \frac{A_1^{\mathrm{u}}}{\gamma\bar{p}_1^{\mathrm{u}}}\right]^T + \mathbf{B}_Q\frac{\hat{\bar{Q}}}{\bar{\dot{Q}}}. \quad (9)$$

According to literature work[17, 18, 24], the transfer function of the swirling flame can be expressed by

$$\frac{\hat{\bar{Q}}}{\bar{\dot{Q}}} = F_{\mathrm{th}}^v(\omega)\left((1-\zeta)\frac{\left(\hat{v}_1^x\right)^{\mathrm{u}}}{\left(\bar{v}_1^x\right)^{\mathrm{u}}} - \chi\frac{\left(\hat{v}_1^\theta\right)^{\mathrm{u}}}{\left(\bar{v}_1^\theta\right)^{\mathrm{u}}}\right), \quad (10)$$

where χ and ζ denote the contributions of azimuthal and axial velocity perturbations. F_{th}^v is the ratio of the relative fluctuation of heat release rate to the relative fluctuations of axial velocity.

Physically speaking, Eq. (6) shows that the axial and azimuthal velocity perturbations are contributed by both the acoustic and vortical disturbances. However, if we consider the axisymmetric case ($m = 0$), which is the basic assumption of the literature work [17, 18, 24], the axial velocity perturbation is solely determined by the acoustic perturbation while the azimuthal velocity perturbation is solely determined by the vortical perturbation. Under such an approximation, Palies et al. [18] gave the following relationship

$$\frac{\left(\hat{v}_1^\theta\right)^{\mathrm{u}}}{\left(\bar{v}_1^\theta\right)^{\mathrm{u}}} = \exp(\mathrm{i}\phi)\frac{\left(\hat{v}_1^x\right)^{\mathrm{u}}}{\left(\bar{v}_1^x\right)^{\mathrm{u}}}. \quad (11)$$

The flame transfer function therefore reduces to

$$\frac{\hat{\bar{Q}}}{\bar{\dot{Q}}} = F_{\mathrm{th}}^v(\omega)\left((1-\zeta) - \chi\exp(\mathrm{i}\phi)\right)\frac{\left(\hat{v}_1^x\right)^{\mathrm{u}}}{\left(\bar{v}_1^x\right)^{\mathrm{u}}}. \quad (12)$$

3. Intrinsic thermoacoustic feedback in swirling flame combustor

As the intrinsic thermoacoustic oscillation can exist in the absence of the reflected waves, we have $P_{1-}^{\mathrm{d}}/\gamma\bar{p}_1^{\mathrm{d}} = P_{1+}^{\mathrm{u}}/\gamma\bar{p}_1^{\mathrm{u}} = 0.$ Furthermore, the entropic perturbation upstream is absent (..). Based on these regulations, Eqs. (8), (11) and (11) can be expressed as $\mathbf{GX} = 0$ with

$$\mathbf{X} = \left[P_{1+}^{\mathrm{d}}/\gamma\bar{p}_1 \quad S_1^{\mathrm{d}}/c_p \quad A_1^{\mathrm{d}}/\gamma\bar{p}_1 \quad P_{1-}^{\mathrm{u}}/\gamma\bar{p}_1 \quad A_1^{\mathrm{u}}/\gamma\bar{p}_1 \quad \hat{\bar{Q}}/\bar{\dot{Q}}\right].$$

Due to the existence of perturbations, we must have $\det(\mathbf{G}) = 0$. After preliminary derivations, we obtain

$$F_{\mathrm{th}}^v(\omega)\left(1 - \zeta - \chi\exp(\mathrm{i}\phi)\right) = -\left(M_1^x\right)^{\mathrm{u}} f, \quad (13)$$

where f is the cofactor in terms of $\hat{\bar{Q}}/\bar{\dot{Q}}$ in $\mathbf{G}$. As we are interested in the effect of ϕ on the critical gain of the intrinsic thermoacoustic oscillation, we do not model the relationship between ϕ and the angular frequency (ω). Introducing the $n-\tau$ model for the transfer function $F_{\mathrm{th}}^v(\omega)$, we have the solution of ω given by

$$\omega = \frac{(2k+1)\pi}{\tau} + \mathrm{i}\frac{1}{\tau}\ln\frac{\left(M_1^x\right)^{\mathrm{u}} f}{n\left(1 - \zeta - \chi\exp(\mathrm{i}\phi)\right)} \quad (14)$$

Clearly, we get the critical gain $n_c = \left|\left(M_1^x\right)^{\mathrm{u}} f \Big/ \left(1 - \zeta - \chi\exp(\mathrm{i}\phi)\right)\right|$ to characterize the stability of the intrinsic oscillations.

Based on the configuration of experimental rig[19, 20], Fig. 2 shows the effects of $\phi \in [0, 2\pi)$ on the critical gain of intrinsic thermoacoustic oscillations meanwhile the model of Courtine et al. [9] for a non-swirling flame. Parameters in the flame transfer function are $\chi = -0.4$ and $\zeta = 0.4$ [18]. Clearly, in the case of $\phi = 0$, the two models nearly coincide. With the increase of ϕ , the critical gain predicted by the present model reflects the effect of ϕ on the intrinsic thermoacoustic oscillation. When ϕ approaches π , the critical gain reaches its maximum. In order to get unsteady

intrinsic thermoacoustic oscillations, the gain of the flame transfer function should be greater than the critical gain according to Courtine et al. [9]. It can be shown that the presence of a swirling flame may therefore stabilize the intrinsic thermoacoustic oscillation by comparing the critical gain between the present model and Courtine's model. Meanwhile, Fig. 3 shows the effects of the cross-sectional area ratio and the base flow velocity upstream on the critical gain of the intrinsic thermoacoustic oscillation.

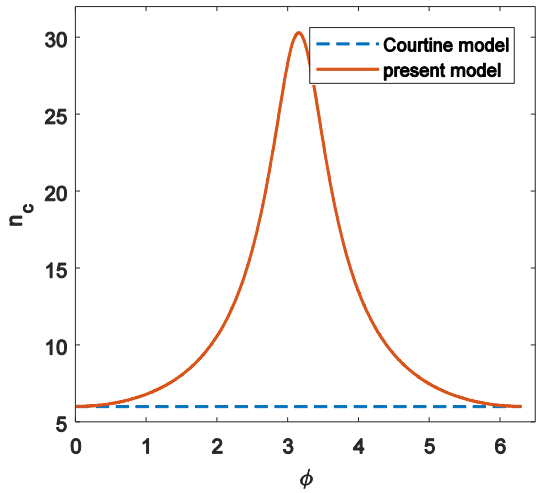

Fig. 2. The effect of ϕ on the critical gain of intrinsic thermoacoustic oscillation.

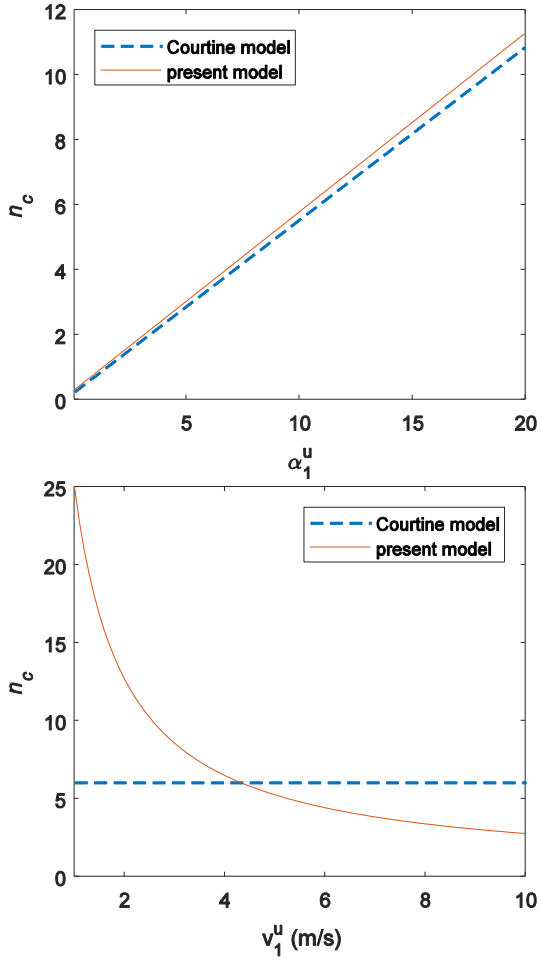

Fig. 3. The effects of cross-sectional area ratio(α_1^u) and base flow velocity upstream on the critical gain of intrinsic thermoacoustic oscillation

In Fig. 3, the phase ϕ in the numerical calculation is $\pi/6$. It can be learned that the effect of cross-sectional area ratio on the critical gain has a similar tendency in the two models. On the other hand, the effect of base flow velocity upstream on the critical gain is different in the two models. As Courtine's model is the zeroth-order approximation in Mach number[25], the predicted critical gain should remain constant despite the variations of the base flow velocity upstream. In the present model, we take into account the first-order approximation in Mach number as shown in Eqs. (1)-(5). With the increase of flow velocity upstream, the critical gain decreases, showing that the possible intrinsic thermoacoustic oscillation may become unsteady. Similar results has been found by Zhao et al. [26].

4. Comparison with literature results

This section compares the theoretical results with experimental studies conducted by Palies et al. [19] and Silva et al. [20]. The corresponding experimental rig, as shown in Fig. 4, consists of three main components, namely a plenum tube, a swirler tube and a combustion chamber.

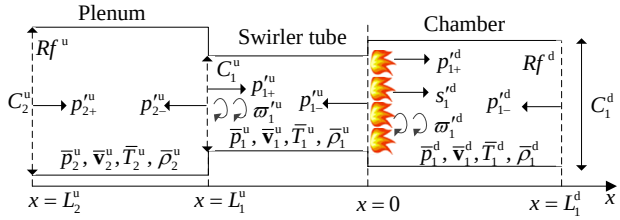

Fig. 4. Schematic of plenum-swirler-chamber system

As the swirler is present and the flame is absent in the swirler tube, the perturbations consist of acoustic and vortical disturbances. From Eq. (8), the perturbation dynamics at location $x = L_1^u$ can be expressed by

$$\begin{bmatrix} \dfrac{\left(\hat{v}_1^u\right)^x}{\left(\bar{v}_1^u\right)^x} & \dfrac{\hat{p}_1^u}{\gamma \bar{p}_1^u} \end{bmatrix} = \mathbf{H}_2^u \begin{bmatrix} \dfrac{\left(\hat{v}_2^u\right)^x}{\left(\bar{v}_2^u\right)^x} & \dfrac{\hat{p}_2^u}{\gamma \bar{p}_2^u} \end{bmatrix}, \ \mathbf{H}_2^u = \begin{bmatrix} 1 & 0 \\ 0 & 1 \end{bmatrix}. \quad (15)$$

Substituting Eq. (11) into the above equation yields

$$\begin{bmatrix} \dfrac{\left(\hat{v}_1^u\right)^x}{\left(\bar{v}_1^u\right)^x} & \dfrac{\hat{p}_1^u}{\gamma \bar{p}_1^u} & \dfrac{\hat{s}_1^u}{c_p} & \dfrac{\left(\hat{v}_1^u\right)^\theta}{\left(\bar{v}_1^u\right)^\theta} \end{bmatrix}^T = \mathbf{H}_2^u \begin{bmatrix} \dfrac{\left(\hat{v}_2^u\right)^x}{\left(\bar{v}_2^u\right)^x} & \dfrac{\hat{p}_2^u}{\gamma \bar{p}_2^u} & \dfrac{\hat{s}_2^u}{c_p} & \dfrac{\left(\hat{v}_2^u\right)^\theta}{\left(\bar{v}_2^u\right)^\theta} \end{bmatrix}^T, \quad (16)$$

with $\mathbf{H}_2^u = \begin{bmatrix} 1 & 0 & 0 & 0 \\ 0 & 1 & 0 & 0 \\ 0 & 0 & 0 & 0 \\ \exp(\mathrm{i}\phi) & 0 & 0 & 0 \end{bmatrix}$. We next consider the dynamics across the flame front in Eq. (9) by combining Eqs. (6) and (16) and get

$$\begin{aligned} &\mathbf{F}_1^u\left(L_1^u\right)\left[\frac{P_{1+}^u}{\gamma \bar{p}_1^u}, \frac{P_{1-}^u}{\gamma \bar{p}_1^u}, \frac{S_1^u}{c_p}, \frac{A_1^u}{\gamma \bar{p}_1^u}\right]^T \\ &= \mathbf{H}_2^u \mathbf{F}_2^u\left(L_1^u\right)\left[\frac{P_{2+}^u}{\gamma \bar{p}_2^u}, \frac{P_{2-}^u}{\gamma \bar{p}_2^u}, \frac{S_2^u}{c_p}, \frac{A_2^u}{\gamma \bar{p}_2^u}\right]^T. \end{aligned} \quad (17)$$

Then Eq. (9) can be expressed as

$$\mathbf{F}_1^{\mathrm{d}}(0)\left[\frac{P_{1+}^{\mathrm{d}}}{\gamma\bar{p}_1^{\mathrm{d}}},\frac{P_{1-}^{\mathrm{d}}}{\gamma\bar{p}_1^{\mathrm{d}}},\frac{S_1^{\mathrm{d}}}{c_p},\frac{A_1^{\mathrm{d}}}{\gamma\bar{p}_1^{\mathrm{d}}}\right]^T = \mathbf{B}_{Sys}\left[\frac{P_{2+}^{\mathrm{u}}}{\gamma\bar{p}_2^{\mathrm{u}}},\frac{P_{2-}^{\mathrm{u}}}{\gamma\bar{p}_2^{\mathrm{u}}},\frac{S_2^{\mathrm{u}}}{c_p},\frac{A_2^{\mathrm{u}}}{\gamma\bar{p}_2^{\mathrm{u}}}\right]^T + \mathbf{B}_Q\frac{\hat{\dot{Q}}}{\bar{\dot{Q}}}, \tag{18}$$

with $\mathbf{B}_{Sys}=\mathbf{H}_1^{\mathrm{u}}\mathbf{F}_1^{\mathrm{u}}(0)\left(\mathbf{F}_1^{\mathrm{u}}\left(L_1^{\mathrm{u}}\right)\right)^{-1}\mathbf{H}_2^{\mathrm{u}}[1\quad 1\quad 0\quad 0]\mathbf{F}_2^{\mathrm{u}}\left(L_1^{\mathrm{u}}\right)$. Substituting Eq. (17) into the flame transfer function (Eq.(10)) gives

$$\left[F_{\mathrm{th}}^{v}(\omega)\left(1-\zeta-\chi\exp(\mathrm{i}\phi)\right)\quad 0\quad 0\quad 0\right]\mathbf{F}_1^{\mathrm{u}}(0)\bullet \left(\mathbf{F}_1^{\mathrm{u}}\left(L_1^{\mathrm{u}}\right)\right)^{-1}\mathbf{H}_2^{\mathrm{u}}\mathbf{F}_2^{\mathrm{u}}\left(L_1^{\mathrm{u}}\right)\left[\frac{P_{2+}^{\mathrm{u}}}{\gamma\bar{p}_2^{\mathrm{u}}},\frac{P_{2-}^{\mathrm{u}}}{\gamma\bar{p}_2^{\mathrm{u}}},\frac{S_2^{\mathrm{u}}}{c_p},\frac{A_2^{\mathrm{u}}}{\gamma\bar{p}_2^{\mathrm{u}}}\right]^T-\frac{\hat{\dot{Q}}}{\bar{\dot{Q}}}=0. \tag{19}$$

We introduce reflection coefficients (Rf^{u} and Rf^{d}) at the upstream and downstream to model the boundary condition. Similarly, we have the following system expression $\mathbf{GX}=0$ with

$$\mathbf{X}=\left[\frac{P_{1+}^{\mathrm{d}}}{\gamma\bar{p}_1}\quad\frac{P_{1-}^{\mathrm{d}}}{\gamma\bar{p}_1}\quad\frac{S_1^{\mathrm{d}}}{c_p}\quad\frac{A_1^{\mathrm{d}}}{\gamma\bar{p}_1}\quad\frac{P_{2+}^{\mathrm{u}}}{\gamma\bar{p}_2}\quad\frac{P_{2-}^{\mathrm{u}}}{\gamma\bar{p}_2}\quad\frac{\hat{\dot{Q}}}{\bar{\dot{Q}}}\right]^T.$$

It should be noticed that the boundary condition downstream only considers the feedback of acoustic perturbations where the effects of vortical and entropic perturbations are neglected. Physically speaking, if the combustor's outlet is choked, these three types of perturbations interact, the reflected pressure perturbation will be excited by the vortical and entropic perturbations. The corresponding boundary condition can be found in Duran and Morgans [27]. As we are interested in the analysis of intrinsic thermoacoustic oscillation, we only consider the acoustic feedback mechanism.

The flame transfer function is adopted from Palies et al. [18] while the axial base flow velocity in the swirler tube is $\bar{v}_1^{\mathrm{u}}=2.67\,\mathrm{m/s}$. In the numerical calculation, ϕ in Eq. (11) is modeled as $\phi=\omega\tau+\phi_0$, where τ represents the transit time difference of acoustic and vortical disturbances propagating to the flame front. Numerous previous studies have shown that the thermoacoustic modes are composed of the purely cavity-based resonant acoustic modes, denoted by "PA", and the intrinsic resonant modes, denoted by "ITA". While the purely cavity-based acoustic modes are decided by the geometries of the combustors, the intrinsic resonant modes are mostly determined by the flame transfer function. In the case of complex geometries as shown in Fig. 3, Albayrak et al. [15] experimentally argued that the ITA frequencies depended not only on the phase of the FTF but also on the flow configurations. In the calculation of ITA criterion, the reflection coefficients upstream and downstream vanishes ($Rf^{\mathrm{u}}=Rf^{\mathrm{d}}=0$), we therefore can calculate the expression of flame transfer function and read

$$F=F_{\mathrm{th}}^{v}(\omega)\left(1-\zeta+\chi\exp(\mathrm{i}\phi)\right)-\xi. \tag{20}$$

Under the configuration of "Flame A" in Palies et al. [18], Fig. 5 shows the gain and phase of the flame transfer function and F where τ and ϕ_0 are 0.012 and -1. The criteria of Albayrak et al. [15], the present model in Eq.(20), and the traditional model written by $F_{\mathrm{th}}^{v}(\omega)\left(1-\zeta+\chi\exp(\mathrm{i}\phi)\right)$ are present simultaneously. Fig. 6 shows the predicted results of thermoacoustic oscillations and the boundary-induced feedback and intrinsic feedback mechanisms. The combustor length (L_1^{d}), swirler-tube length($\left|L_1^{\mathrm{u}}\right|$) and plenum length ($\left|L_2^{\mathrm{u}}-L_1^{\mathrm{u}}\right|$) in the numerical calculation are 0.4m, 0.1167m, and 0.1888. In Fig. 5, thermoacoustic modes of the whole system, where the flame unsteady heat release rate and the boundary reflection are present, are denoted by 'TA'.

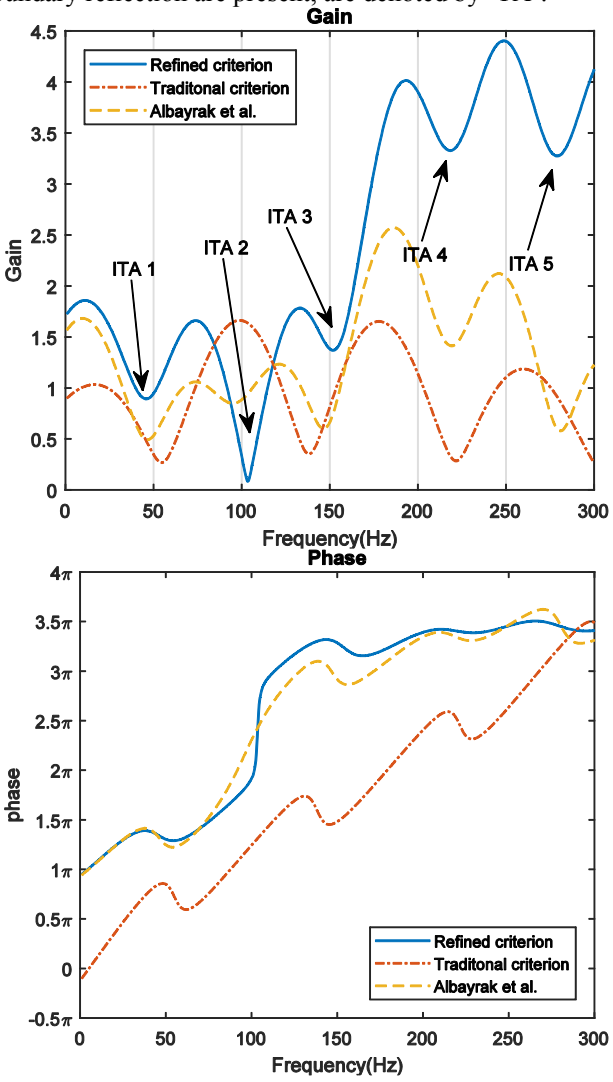

Fig. 5. Gain and phase of different types of ITA criteria

Fig. 5 shows that there are 5 local minimum values of the refined criterion, which means that the system has 5 ITA modes. Fig. 6 confirms the predictions. Interestingly, Fig. 4b shows that these five ITA modes don't correspond to an odd multiple of π . Furthermore, these ITA modes are not determined by traditional $-\pi$ criterion. The ITA modes predicted by the present model, within acceptable error, are consistent with the prediction made by the criterion of Albayrak et al. [15]. Interestingly, the phase of the present

model has very similar tendencies to that from the model of Albayrak et al. [15].

Palies et al. [19] reported that there was an unstable mode near 116Hz, which is also recovered by the present model as shown by 'TA 3' in Fig. 5. Palies et al. [19] extended to analyze its characteristics under the effect of nonlinear flame describing function. The present paper tries to analyze the relationship between TA modes with ITA and PA feedback mechanisms, the nonlinear effects are therefore omitted. According to the previous work [25], we find that this unstable mode comes from the PA mode in terms of the Helmholtz resonator constructed by the plenum and swirl-tube. Chen and Driscoll [28] showed that the frequency of the Helmholtz resonator could be roughly calculated through $\bar{c}_2^{\mathrm{u}}/2\pi\sqrt{\left(C_1^{\mathrm{u}}/C_2^{\mathrm{u}}\right)/\left(L_1^{\mathrm{u}}\left(L_2^{\mathrm{u}}-L_1^{\mathrm{u}}\right)\right)}\approx 121.24\,\mathrm{Hz}$.

Fig. 6 shows the predicted results of thermoacoustic oscillations and the boundary-induced feedback and intrinsic feedback mechanisms. The combustor length, swirler-tube length and plenum length in the numerical calculation are 0.4m, 0.1167m, and 0.1888. In Fig. 6, thermoacoustic modes of the whole system, where the flame unsteady heat release rate and the boundary reflection are present, are denoted by 'TA' and the intrinsic thermoacoustic modes, where the flame unsteady heat release rate is present but the boundary reflections downstream and upstream are absent, are denoted by 'ITA'. The reflection-induced cavity acoustic mode is denoted by 'PA' without the presence of the unsteady heat release rate.

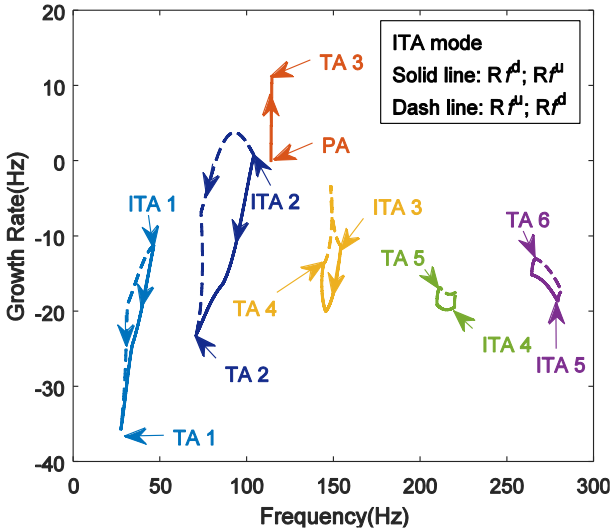

Fig. 6. Modes predictions of thermoacoustic oscillations in the test rig.

Palies et al. [19] reported that there was an unstable mode near 116Hz, which is also recovered by present model as shown by 'TA 1' in Fig. 6. Palies et al. [19] extended to analyze its characteristics under the effect of nonlinear flame describing function. The present paper tries to analyze the relationship between TA modes with ITA and PA feedback mechanisms, the nonlinear effects are therefore omitted. From previous work[25], we find that this unstable mode comes from the PA mode in terms of the Helmholtz resonator constructed by the plenum and swirl-tube. Chen and Driscoll [28] shows that the frequency of the Helmholtz resonator can be roughly determined by $\bar{c}_2^{\mathrm{u}}/2\pi\sqrt{\left(C_1^{\mathrm{u}}/C_2^{\mathrm{u}}\right)/\left(L_1^{\mathrm{u}}\left(L_2^{\mathrm{u}}-L_1^{\mathrm{u}}\right)\right)}\approx 121.24\,\mathrm{Hz}$.

As we are interested in the evolution mechanism from Helmholtz resonance to the thermoacoustic oscillation, we multiply the right hand side of Eq. (10) with a factor β to control the amplitude of the flame. Specifically, the condition of $\beta=0$ means the absence of the burner meanwhile the condition of $\beta=1$ means the original flame transfer function in Eq. (10) is taken into effect. The orbit from 'PA' to 'TA 3', which is denoted by an arrow in Fig. 6, is calculated by increasing the factor β from 0 to 1. From this orbit, we see that the effect of the unsteady heat release rate mainly changes the growth rate and has limited influence on the resonant frequency. The five ITA modes, found in Fig. 6, are shown to be stable. The frequencies of these ITA modes are roughly 45Hz, 100Hz, 150Hz, 220Hz, and 278Hz, which approximately replicate the locations of local minima of the gain in Fig. 5.

As we are interested in the evolution from the ITA modes to the corresponding TA modes, we introduce two different strategies to track the evolution orbits by solid and dashed lines in Fig. 5. Meanwhile, the involution directions in the two strategies are denoted by arrows. Specifically, the evolution orbit by the solid line is calculated by firstly changing gradually the boundary condition at the outlet of the chamber from the anechoic condition ($Rf^{\mathrm{d}}=0$) to the fully reflecting condition ($Rf^{\mathrm{d}}=-1$), meanwhile the boundary condition at the inlet of the plenum remain anechoic ($Rf^{\mathrm{u}}=0$). Secondly, we gradually change the inlet of the plenum from the anechoic condition ($Rf^{\mathrm{u}}=0$) to the fully reflecting condition ($Rf^{\mathrm{u}}=1$) meanwhile the boundary condition at the outlet of the chamber keep reflected ($Rf^{\mathrm{d}}=-1$). The evolution orbit by the dashed line is calculated by the opposite order. Roughly speaking, we firstly change the boundary condition at the outlet of the chamber from the anechoic condition to the reflecting condition under the anechoic condition of the inlet of the plenum. Secondly, we change the boundary condition at the inlet of the plenum from the anechoic condition to the fully reflecting condition under the configuration of a reflecting condition at the inlet of the plenum. The common features of these dispersions are that the frequency of the TA mode is smaller than the corresponding ITA mode. Furthermore, the reflection coefficient on the growth rate is complicated for each mode. It can be learned that the solid and dashed lines give the boundaries which regulate possible evolution orbits. The fact that these lines do not intersect indicates that the ITA and PA modes will independently evolve to their corresponding TA mode, which constitutes the oscillation distribution of the whole system.

Fig. 7 shows the effect of transit time difference τ in $\phi=\omega\tau+\phi_0$ on the ITA modes and ITA-induced TA modes of the system with τ ranging from 0 to 0.2 and ϕ_0 being -1. Fig. 8 shows the transit time difference on the PA-induced

TA modes. Fig. 7 shows the evolution dispersion of the PA-induced TA mode. The arrow in each line represents the corresponding evolution direction. Physically speaking, in the axisymmetric approximation (the azimuthal wavenumber is $m=0$), τ is the difference of the transit time between acoustic and vortical perturbations due to different propagation speeds, which can represent the effects of the swirler location, denoted by $x=x_2$ in Fig. 4, and the axial base flow velocity ($\bar{v}^x$), due to the fact that the vortical perturbation is convected with the flow velocity, on the oscillations in the system. Han and Hochgreb [29] gave its mathematical modelling for a stratified swirling flame and showed that the transit time difference is determined by the swirler location in the swirler tube. In this paper, we directly consider the transit time difference instead of the swirler location.

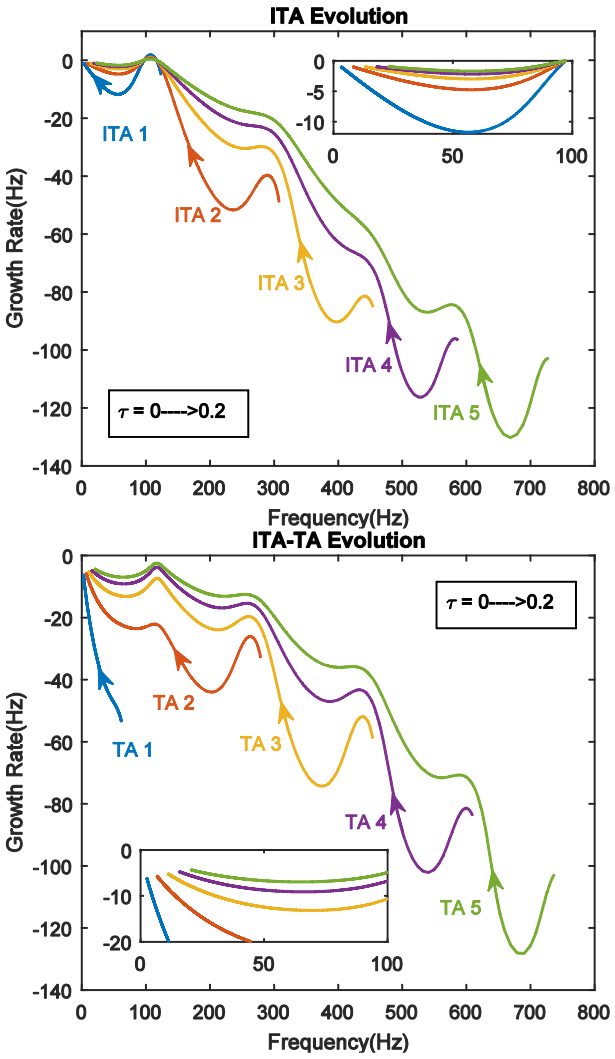

Fig. 7. Evolution orbits of thermoacoustic modes and intrinsic modes due to the variation of τ.

The Helmholtz-induced TA3 mode remains unstable during the change of τ as shown in Fig. 7. Interestingly, the dynamics of the PA-induced TA mode behave as a periodic orbit. With the increase of τ, which reveals the increase of the distance from the flame location to the swirler location or the decrease of the convected flow velocity of the vortical perturbation ($\bar{v}^x$), the induced TA mode asymptotically approaches to an attractor (116, 10.47) as shown in Fig. 7.

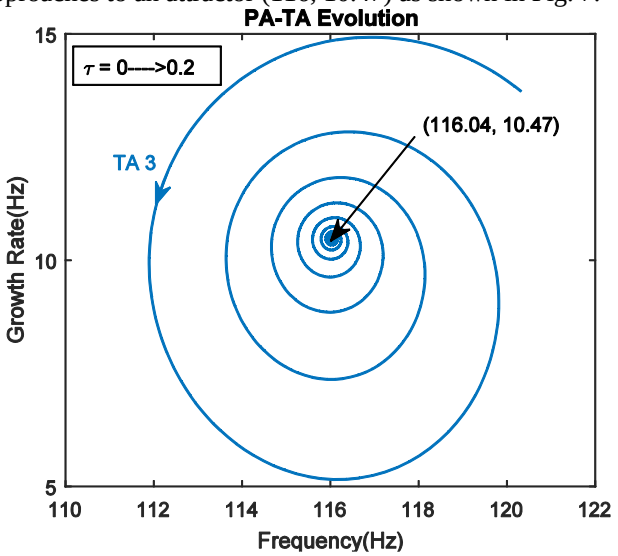

Fig. 8. PA-induced thermoacoustic oscillation affected by the phase shift of the swirling flame

5. Conclusions

This paper gives a comprehensive derivation of the two dimensional azimuthal-axial perturbations for a swirling flame, the dynamics of acoustic, entropic and vortical perturbations generated by the unsteady heat release rate are given in section 2. Similar to intrinsic-induced longitudinal combustion instabilities [5, 9], the critical gain of the intrinsic thermoacoustic oscillation is derived and a parametric analysis is given in section 3. It shows that the difference of the transit phase between vortical and acoustic perturbations imposes great influence on the critical gain of ITA oscillations.

Based on the configuration of the plenum-swirler-chamber combustor by Palies et al. [20] and Silva et al. [21], analytical prediction by the present work match well with the results by Palies et al. [20]. By analyzing the evolution dispersion of theta modes, the present work confirms that the TA oscillations of a system are composed of the ITA and PA feedback mechanisms, which have independent evolution features as shown in Fig. 5. The phase shift (denoted by τ) due to different propagating speeds of the axial and azimuthal velocity perturbations play significant influence on both the ITA and PA feedback mechanisms. Specifically, with the increase of τ, the PA-induced TA oscillation asymptotically converges to the condition that the vortical perturbation can be omitted with $\chi=0$.

References

[1] T.C. Lieuwen, Modeling premixed combustion-acoustic wave interactions: a review, *J. Propul. Power* 19 (5) (2003) 765-781.

[2] T. Poinsot, Prediction and control of combustion instabilities in real engines, *Proc. Combust. Inst.* 36 (2017) 1-28.

[3] A.P. Dowling, Y. Mahmoudi, Combustion noise, *Proc. Combust. Inst.* 35 (2015) 65-100.

[4] T. Poinsot, D. Veynante, Theoretical and numerical combustion, Edwards, United State of America, 2005.

[5] M. Hoeijmakers, V. Kornilov, I.L. Arteaga, P.d. Goey, H. Nijmeijer, Intrinsic instability of flame–acoustic coupling, *Combust. Flame* 161 (2014) 2860-2867.
[6] T. Emmert, S. Bomberg, W. Polifke, Intrinsic thermoacoustic instability of premixed flames, *Combust. Flame* 162 (2015) 75-85.
[7] S. Bomberg, T. Emmert, W. Polifke, Thermal versus acoustic response of velocity sensitive premixed flames, *Proc. Combust. Inst.* 35 (2015) 3185-3192.
[8] N.K. Mukherjee, V. Shrira, Intrinsic flame instabilities in combustors: analytic description of a 1-D resonator model, *Combust. Flame* 185 (2017) 188-209.
[9] E. Courtine, L. Selle, T. Poinsot, DNS of Intrinsic ThermoAcoustic modes in laminar premixed flames, *Combust. Flame* 162 (2015) 4331-4341.
[10] C.F. Silva, T. Emmert, S. Jaensch, W. Polifke, Numerical study on intrinsic thermoacoustic instability of a laminar premixed flame, *Combust. Flame* 162 (2015) 3370-3378.
[11] C.F. Silva, M. Merk, T. Komarek, W. Polifke, The contribution of intrinsic thermoacoustic feedback to combustion noise and resonances of a confined turbulent premixed flame, *Combust. Flame* 182 (2017) 269-278.
[12] M. Hoeijmakers, V. Kornilov, I.L. Arteaga, P.d. Goey, H. Nijmeijer, Flame dominated thermoacoustic instabilities in a system with high acoustic losses, *Combust. Flame* 169 (2016) 209-215.
[13] N. Hosseini, V. Kornilov, L. Arteaga, W. Polifke, O. Teerling, L.d. Goey, Intrinsic thermoacoustic modes and their interplay with acoustic modes in a Rijke burner, *International Journal of Spray an Combustion Dynamics* 10 (4) (2018) 315-325.
[14] T. Emmert, S. Bomberg, S. Jaensch, W. Polifke, Acoustic and intrinsic thermoacoustic modes of a premixed combustor, *Proc. Combust. Inst.* 36 (2017) 3835-3842.
[15] A. Albayrak, T. Steinbacher, T. Komarek, W. Polifke, Convective scaling of intrinsic thermo-acoustic eigenfrequencies of a premixed swirl combustor, *J. Eng. Gas Turbines Power.* 140 (4) (2018).
[16] M. Murugesan, B. Singaravelu, A.K. Kushwaha, S. Mariappan, Onset of flame-intrinsic thermoacoustic instabilities in partially premixed turbulent combustors, *Int. J. Spray Combust.* 10 (3) (2018) 171-184.
[17] S. Candel, D. Durox, T. Schuller, J.-F. Bourgouin, J.P. Moeck, Dynamics of swirling flames, *Annu. Rev. Fluid Mech.* 46 (2014) 147-173.
[18] P. Palies, T. Schuller, D. Durox, S. Candel, Modeling of premixed swirling flames transfer functions, *Proc. Combust. Inst.* 33 (2011) 2967-2974.
[19] P. Palies, D. Durox, T. Schuller, S. Candel, Nonlinear combustion instability analysis based on the flame describing function applied to turbulent premixed swirling flames, *Combust. Flame* 158 (2011) 1980-1991.
[20] C.F. Silva, F. Nicoud, T. Schuller, D. Durox, S. Candel, Combining a Helmholtz solver with the flame describing function to assess combustion instability in a premixed swirled combustor, *Combust. Flame* 160 (2013) 1743-1754.
[21] S.R. Stow, A.P. Dowling, Thermoacoustic oscillations in an annular combustor, Proceedings of ASME TURBO EXPO, 2001, 2001-GT-0037.
[22] R.J. LeVeque, Numerical methods for conservation laws, Birkhauser Verlag, Boston, 1992.
[23] U.T. Joyner, Charts of pressure, density, and temperature changes at an abrupt increase in cross-sectional area of flow of compresssible air, Report, No. 1945.
[24] P. Palies, D. Durox, T. Schuller, S. Candel, The combined dynamics of swirler and turbulent premixed swirling flames, *Combust. Flame* 157 (9) (2010) 1698-1717.
[25] Y. Chen, L.J. Ayton, D. Zhao, Modelling of intrinsic thermoacoustic instability of premixed flame in a nonuniform-radius combustor, *Combust. Sci. Technol.* (2019).
[26] D. Zhao, S. Li, H. Zhao, Entropy-involved energy measure study of intrinsic thermoacoustic oscillations, *Appl. Energy* 177 (2016) 570-578.
[27] I. Duran, A.S. Morgans, On the reflection and transmission of circumferential waves through nozzles, *J. Fluid Mech.* 773 (2015) 137-153.
[28] Y. Chen, J.F. Driscoll, A multi-chamber model of combustion instabilities and its assessment using kilohertz laser diagnostics in a gas turbine model combustor, *Combust. Flame* 174 (2016) 120-137.
[29] Z. Han, S. Hochgreb, The response of stratified swirling flames to acoustic forcing: experiments and comparison to model, *Proc. Combust. Inst.* 35 (2015) 3309-3315.